https://doi.org/10.2352/issn.2169-2629.2021.29.31

Investigating the Kokhanovsky snow reflectance model in close-range spectral imaging

Mathieu Nguyen, Jean-Baptiste Thomas, Ivar Farup; Department of Computer Science, Norwegian University of Science and Technology; Gjøvik, Norway

Abstract

The internal structure of the snow and its reflectance function play a major contribution in its appearance. We investigate the snow reflectance model introduced by Kokhanovsky and Zege in a close-range imaging scale. By monitoring the evolution of melting snow through time using hyperspectral cameras in a laboratory, we estimate snow grain sizes from 0.24 to 8.49 mm depending on the grain shape assumption chosen. Using our experimental results, we observe differences in the reconstructed reflectance spectra with the model regarding the spectra's shape or magnitude. Those variations may be due to our data or to the grain shape assumption of the model. We introduce an effective parameter describing both the snow grain size and the snow grain shape, to give us the opportunity to select the adapted assumption. The computational technique is ready, but more ground truths are required to validate the model.

Introduction

Stating that snow is white would be a good simplification of a sophisticated and complex phenomenon. During a sunny day, it is possible to see green or yellow sparkles on a snow landscape. At night, under natural or artificial light sources, snow appears to be gray or blue if shadows are cast on the scene. Many phenomena are at stake and will influence the way snow is perceived. The grain size and the grain shape define the structure of the snow, thus defining the optical characteristics of the snow: absorption, refraction and scattering. Furthermore, snowpacks can be organized as snow layers impacting the light propagation [14], and can contain pollutants influencing its optical characteristics [1].

In this work, we investigate those parameters with a snow reflectance model established by Kokhanovsky and Zege [11] using hyperspectral images. This model has been widely studied for the last 15 years. It was compared to in-situ measurements by Kokhanovsky et al. [8], and later on, approved using multi-angular and multispectral observations over Greenland and Antartica [9]. It has also been used in the remote sensing area for retrieval or estimation of snow grain size [2, 19]. Others have used the exponential model of the snow reflectance function with near-infrared (NIR) and short-wave infrared (SWIR) photographies to measure the snow specific surface area (SSA). Gallet et al. [4] used an integrating sphere to measure the SSA at 1310 and 1550 nm. Another method was used by Langlois et al. [13], Matzl and Shneebeli [15] and Montpetit et al. [17] as they all measured the SSA using in-situ hyperspectral photographies of snow pits and snow walls.

Although the Kokhanovsky model has been thoroughly tested for the remote sensing setting, it is not well understood how it performs for close-range imaging. Coupled with hyperspectral cameras, we use the reflectance model to estimate the snow grain size and the concentration of pollutants of a snow sample in laboratory. Since obtaining a proper value of the grain size is subject to a choice of assumption on the grain shape, we introduce an effective parameter to better qualify the snow.

The first section of this article presents the snow reflectance model along with the refractive indices used. A short study on the influence of studied parameters is conducted as well. In a second section, the methodology of our experimental acquisition is introduced along with the model inversion used. The third section highlights the main results and discussion of that study, followed by a conclusion and future works.

Snow reflectance

In this section, we chose to present a snow reflectance model based on the work of Kokhanovsky and Zege [11] over other models for its simplicity and small number of parameters, which permits its inversion and the retrieval of the parameters with limited struggle. Following the reflectance model are the refractive indices used extracted from Warren et al. [22], and an influence study of the parameters in the Kokhanovsky model.

Kokhanovsky snow reflectance model

One way of modeling the reflectance function is to solve the radiative transfer equation (RTE) that describes the propagation of light inside materials. As described in [11], it requires some assumptions to obtain an asymptotic solution to the RTE. The major assumptions are: snow has an infinite thickness (ie. no contribution of what is below the snow layers), snow grains have little absorption of light and the light coming from the source is azimuth independent. The RTE is defined by Equation (1):

$$\mu \frac{\partial I(\tau,\mu,\phi)}{\partial \tau} = I(\tau,\mu,\phi) - S(\tau,\mu,\phi) \tag{1}$$

where I is the specific intensity, S is the source function (therefore independent of the azimuth ϕ by assumption in our case), τ is the optical length and μ is the cosine of the polar angle. Therefore, following the previous assumptions established and the derivations detailed in [7], the snow reflectance function can be modeled by Equation (2):

$$R(\lambda,\theta_0,\theta,\varphi) = R_0(\theta_0,\theta,\varphi)\exp\Big(-\frac{K(\theta)K(\theta_0)}{R_0(\theta_0,\theta,\varphi)} b\sqrt{d\gamma(\lambda)}\Big), \tag{2}$$

where R represents the bidirectional function (also known as the Bidirectional Reflectance Distribution Function or BRDF) for the reflectance under the assumption of a semi-infinite layer and R_0 is the value of R at zero absorption (equation given in [7]).

The parameters $(\theta_0,\theta,\varphi)$ describe the geometry of the situation studied by respectively being the incident illumination angle of the light source, the viewing angle for the observation system, and the relative azimuth between the source and the viewing system. All those angles are given in degrees. $K(\theta)$ is called the escape function, and is defined in Milne's problem

[16]. Under the assumption of $\cos\theta \geq 0.2$ (corresponding to $\theta \leq 75°$), excluding grazing angles, we can approximate $K(\theta)$ by $K(\theta) = \frac{3}{7}(1+2\cos\theta)$ [10].

The parameter b is defined as the shape factor and represents the influence of the shape of snow grains. Several shapes are reported in the literature [3], and their characteristics impact the propagation of light. Kokhanovsky and Zege [11] established their model under the assumption of a fractal grain shape, giving the value of $b = 3.62$. That assumption will be discussed later in the results and discussion section. The parameter d stands for the snow grain size and is given in micrometers. Its definition has long been debated: some authors considered it as the diameter of a spherical snow grain [18, 11], other as the greatest dimension of a snow grain [1]. This is also the parameter that could be linked to the SSA [17].

$\gamma(\lambda)$ is the coefficient of absorption of the medium, which is defined by Equation (3):

$$\gamma(\lambda) = \frac{4\pi}{\lambda}(\chi(\lambda)+M), \tag{3}$$

where λ is the wavelength of light in nanometers, $\chi(\lambda)$ the imaginary part of the refractive index of the medium considered, and M the concentration of pollutants in the medium [1, 9].

In our context, we are studying the spectra of VNIR and SWIR images. Therefore, the wavelength is a varying parameter whereas the lighting and observing conditions are known (ie. we are not in a goniometric study). Thus, we discard the dependence on $(\theta_0, \theta, \varphi)$ and we can rewrite Equation (2) into

$$R(\lambda) = R_0 \exp\Big(-\alpha b\sqrt{d}\sqrt{\frac{(\chi(\lambda)+M)}{\lambda}}\Big) \tag{4}$$

with $\alpha = \frac{K(\theta)K(\theta_0)}{R_0}\sqrt{4\pi}$ being a known constant.

Refractive index

Refractive indices have a major role in understanding the optical behavior of a material. For our case, our interest is solely focused on the imaginary part of the refractive index, as it is linked to the absorption of a medium in the electromagnetic theory. Also, as we are studying the evolution of snow along time as it melts away, it is safe to assume a mixture of ice and water.

For describing snow in the wavelength range of 400 nm to 2500 nm, few databases are available for the imaginary part of the refractive index. Hale et al. [5] are providing measurements of the water refractive index for water samples at a temperature of 25°C. Warren [22] established a compilation of refractive indices in the case of ice, and a revision to that database was given later [23] with changes in the range 1400 nm to 1800 nm for our interest. Both references are actually doing a compilation of several experimental results obtained by other authors with smoothing and linear interpolation when necessary. Kou et al. [12] have done measurements on their side and compared them to those of Hale et al. for the water, and Warren for the ice. They noted small differences for some wavelengths but since general results are quite similar, those databases can be trusted to a certain degree.

Influence of parameters (grain size and pollutant coefficient)

Sources of pollution are most likely soot, dust or new deposited snow on top of the snowpack. Aoki et al. [1] were one of the first to lead a study on the influence of both the grain size and the concentration of pollutants in the snow in the NIR range. Their study showed promising results and was later reiterated by using hyperspectral satellites in remote sensing [9] or by using contact spectroscopy directly on the field [21]. In Equation (4), the parameters at stake are the snow grain size d and the concentration of pollutants M. Then, we used the database of Warren [22] for the ice refractive indices to observe the influence of those parameters. Results obtained in Figures 2 and 3 are under the fractal assumption for the snow grain shape (ie. b = 3.62 in [11]). For the geometrical configuration, we used $(\theta_0, \theta, \varphi) = (45°, 0°, 0°)$ as it is the configuration we had for our experiment. In this case, the value of R_0 is $R_0 = 1.035$ (obtained from Equations (4) and (11) in [6]).

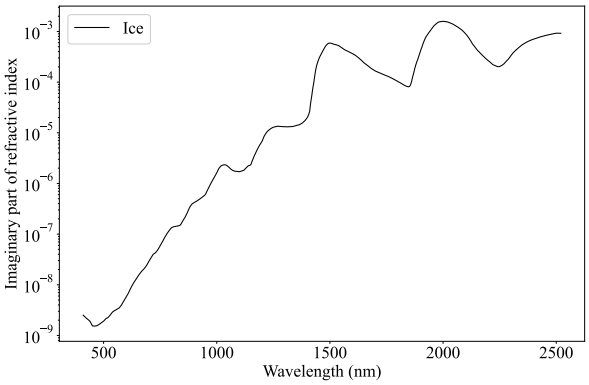

Figure 1. *Evolution of the imaginary part of the ice refractive index based on the database in [22]. The y-axis is displayed in logarithmic scale.*

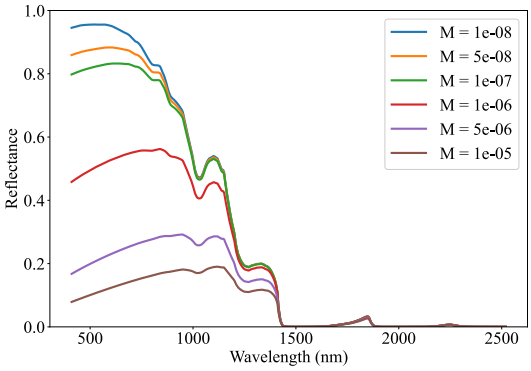

Figure 2. *Influence of the concentration of pollutants for a grain size of 1000 µm.*

On Figure 2, at a fixed value of snow grain size (d = 1000 µm) and for an increasing concentration of pollutants, the reflectance curve is tilted away in the visible range but is still conserving characteristic responses at bands 1050 nm, 1300 nm, 1800 nm and 2300 nm. That result is coherent with the work of Singh et al. [21] who showed that the concentration of pollutants had more impact on the visible reflectance of the snow rather than on the NIR or SWIR. On Figure 1 is plotted the evolution of the imaginary part of the ice refractive index used for the computation of the model. Linking those values with Figure 2, for some wavelengths, M is negligible in front of $\chi(\lambda)$ thus explaining some saturations visible for certain bands. For Figure 3, the evolution of the snow grain size clearly changes the magnitude of the reflectance of the snow. It is more observable in the visible range since the reflectance values are higher than

in the SWIR range from the beginning, but the decrease is quite homogeneous.

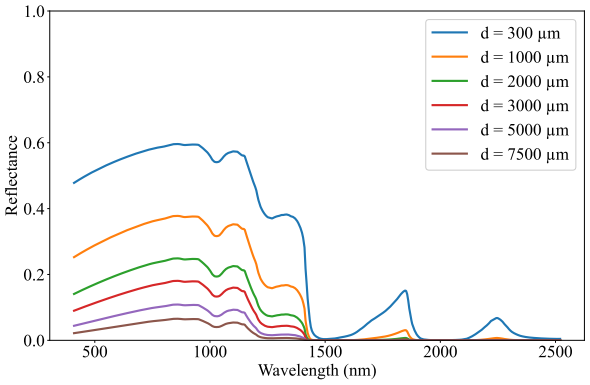

Figure 3. *Influence of the snow grain size for a concentration of pollutants of* 3.10^{-6}

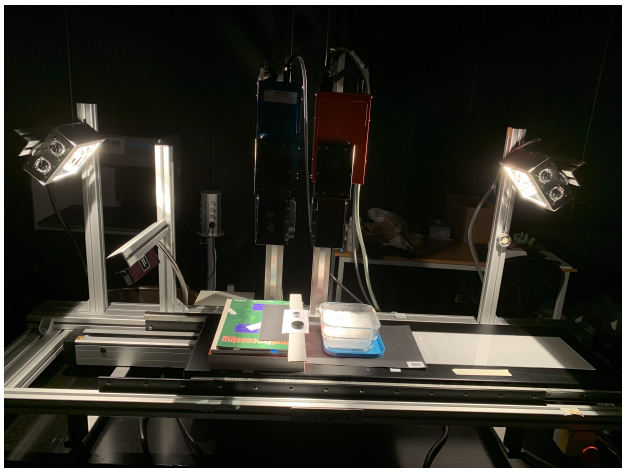

Figure 4. *Experimental setup for the acquisition. The Spectralon® and the snow sample are placed on a moving platform whose speed is controlled by a computer and linked to the integration time of each camera. The platform is moving from right to left on this picture.*

Methodology

Our ultimate focus is to observe the snow grain sizes of snow layers by using hyperspectral images. However, due to the complexity of going outside with our equipement, we decided to study the evolution of the snow grain size through time while the snow sample is melting. We expect an increase of the grain size with time. This was an alternative to the snow layers study that was achievable in a laboratory where light conditions can be controlled. The resulting images were the basis for the computation of spectra and reconstruction of the reflectance functions. Then, a model inversion was run to have an estimate of parameters such as the snow grain size and the concentration of pollutants.

Acquisition process

For this acquisition, we had two hyperspectral cameras at our disposal. The first one is the HySpex VNIR-1800 with 186 bands from 400 nm to 1000 nm with a spectral resolution of 3.17 nm. The second camera is the HySpex SWIR-384 with 288 bands from 950 nm to 2500 nm with a spectral resolution of 5.43 nm. Both cameras are sharing an overlap of bands that will be useful later to connect the spectra obtained from each camera. For this experiment, we used a reference object called Spectralon® to compute the reflectance of snow. The Spectralon® is a white surface whose reflectance function is known for a specific range of wavelengths. So, when setting up the experiment, we calibrate the integration time on the Spectralon®.

The setup of the experiment can be seen on Figure 4. We used two identical lights provided with the cameras that allowed us to have an illumination response in the infrared. Those lights were placed so that the incident angle on the snow would be $\theta_0 = 45°$ for each camera, and the viewing angle would be $\theta = 0°$. The value of the relative azimuth ϕ is of less importance because the cameras are orthogonal to the scene. For both cameras, the integration times were tuned independently. They were chosen so that the illumination of the Spectralon® was around 50% in each images for VNIR and SWIR. On Figure 4, one may note some light pollutions. It does not have a major impact on the model since illuminations angles remain constant. Furthermore, it was a strategic choice to avoid doing two scans for both camera. That way, the acquisitions for the VNIR and SWIR are very close in time and with no changes in the snow sample.

The snow sample used was mainly composed of snow taken outside of our laboratory and put in a glass box. The transportation was done with an isothermic bag to minimize thermal exchanges. That experiment was conducted in late March in Norway with temperature close to 0°C at that time. Unfortunately, we were not able to conduct any chemical analysis of the sample to determine the concentration of pollutants. With the snow sample, we were able to acquire 17 images for both camera in a span or 2 hours. The transformation of solid snow into liquid water was clearly visible on the last spectral images.

Reconstruction of the full spectrum

From the previous acquisition are obtained 34 images in total, 17 for each camera. Figure 5 shows an image from the VNIR camera (left) taken for the band 663 nm, and an image from the SWIR camera (right) taken at 1388 nm (wavelengths chosen for their contrast and showing purposes). Also, both images were acquired at the beginning of the experiment (0 min) when the snow was the freshier.

In the process for the reconstruction of VNIR and SWIR spectrum, we selected two areas of pixels: one focused on the Spectralon® used as a reference I_{ref}, and a second area focused on the snow sample I_{snow}. The main challenge was to ensure the area of the snow would remain the same across time and that we would be looking at the same material on the 17 images. This was quite difficult as the snow is turning into liquid water, leading to small unpredictable translations and rotations. Once those regions of interest defined, and knowing the reflectance of the Spectralon® tile $f_{spec}(\lambda)$, the reflectance function can be reconstructed following Equation (5):

$$R(\lambda) = \frac{I_{snow}}{I_{ref}} f_{spec}(\lambda) \tag{5}$$

which gives us the spectrum of the VNIR camera and the spectrum of the SWIR camera.

To assemble the two spectra obtained from the VNIR and the SWIR images, we used the shared overlap of bands between 950 nm and 1000 nm, assuming linearity of the cameras. Since both cameras do not have the same spectral resolution (the VNIR is at 3.17 nm and the SWIR at 5.43 nm), a resample around 3 nm by linear interpolation was required to compute a scaling factor between the two data. The ratio computed was the VNIR over the SWIR, and we took the average from each band from 950 nm to 1000 nm. Therefore, to obtain spectra such as Figure 6 for each

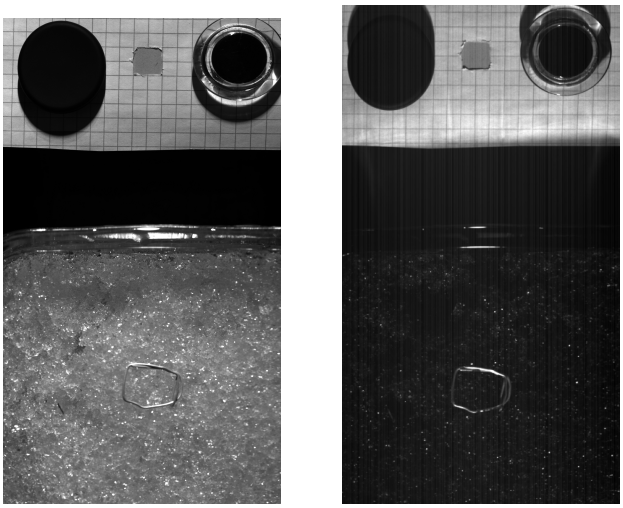

Figure 5. *Examples of images obtained from the VNIR (left, at 663 nm) and the SWIR (right, at 1388 nm) cameras. The Spectralon® reference is on the top of images (square target in the paper sheet between the two magnets), and the snow target on the bottom. Those images are taken at the beginning of the experiment.*

image sets, we multiplied the SWIR data by the ratio computed and we connected the VNIR and SWIR data. We chose that ratio because the data in the SWIR range have a magnitude lower than the VNIR data, so they would not be much affected by the scaling factor.

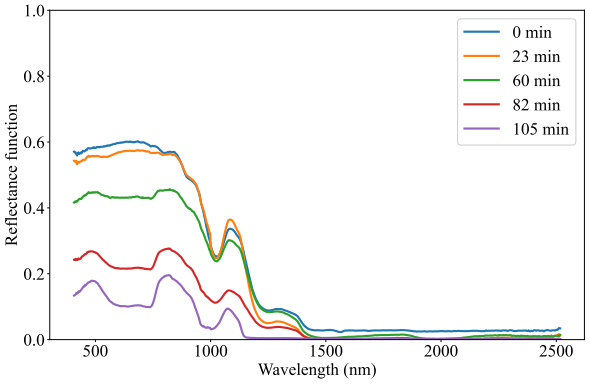

Figure 6. *Full spectrum reconstructed for a couple of images along the experiment. The VNIR and SWIR spectra were connected using the shared overlap between 950 nm and 1000 nm.*

Model inversion

Once the full spectrum is reconstructed, we can focus on the estimation of the snow grain size and the concentration of the pollutants. We rewrite the Equation (4) under Equation (6):

$$R_{\beta,M}(\lambda) = R_0 \exp\Big(-\alpha\beta\sqrt{\frac{(\chi(\lambda)+M)}{\lambda}}\Big) \tag{6}$$

with $\beta = b\sqrt{d}$ and M as parameters to estimate. We chose to look at the product β and not only the snow grain size d since b is chosen under an assumption of the snow grain shape. Therefore, we are optimizing the product containing the information of the snow grain (both shape and size) and we just have to choose one assumption to have an estimate of d.

For this model inversion of the spectrum reconstructed $y(\lambda)$, we chose two costs functions:

$$C_1 = ||R_{\beta,M}(\lambda) - y(\lambda)||_F \tag{7}$$

and

$$C_2 = \cos^{-1}\Big(\frac{\sum_i y_i(\lambda) R_{\beta,M}(\lambda)_i}{||y(\lambda)||_F ||R_{\beta,M}(\lambda)||_F}\Big) \tag{8}$$

with $||A||_F = \sqrt{\sum_i (a_i)^2}$ known as the Frobenius norm, and C_2 is the Spectral Angle Mapper (SAM). Note that SAM is not affected by the scaling choice of the reflectance, which is one of the reasons we chose that cost function. Therefore, the estimate of $(\hat{\beta},\hat{M})$ is given by

$$(\hat{\beta},\hat{M}) = \arg\min_{\beta,M} \mathscr{C}_{1,2} \tag{9}$$

The optimizer used for that study is an optimizer of Nelder-Mead. To ensure that we were not at a local minimum, several seeds were tested for that optimizer and the results were always the same. Furthermore, we also computed some global optimization using dual annealing and we found the same results as with the Nelder-Mead.

Results and Discussion

We used the spectral data acquired and compared it to the model introduced earlier in order to estimate the snow grain size through the parameter β and the concentration of pollutants in the snow M. In doing so, two approaches were taken:

- Approach 1 consisted in estimating both parameters at the same time using Equation (9). That approach gave us values of β and M for each acquisition along time. It is labelled C1-1 and C2-1 for the use of cost functions C_1 and C_2 in the following figures.
- In approach 2, both parameters were estimated from the first acquisition at $t = 0$ min, and the value of M found was kept for the rest of the inversion to only have one parameter to estimate. We argue that the concentration of pollutants is not expected to change with the snow melting. Similarly as the approach 1, it is labelled C1-2 and C2-2.

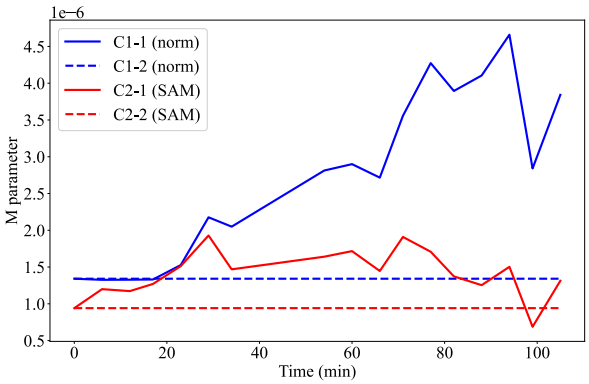

Figure 7. *Estimation of M parameter using the two cost functions $\mathscr{C}_1$ and $\mathscr{C}_2$ with the first approach of optimization.*

Results for the M parameter are displayed on Figure 7. In the first approach, C_1 gives an increasing estimate with time while C_2 provides an estimate in a narrower range. That result

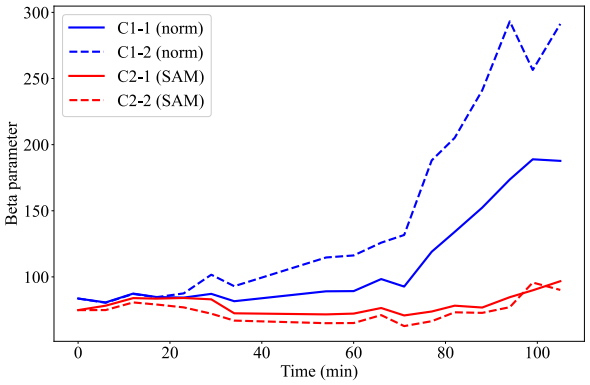

Figure 8. *Estimation of β parameter using the two cost functions $\mathscr{C}_1$ and $\mathscr{C}_2$ with two approaches of optimization.*

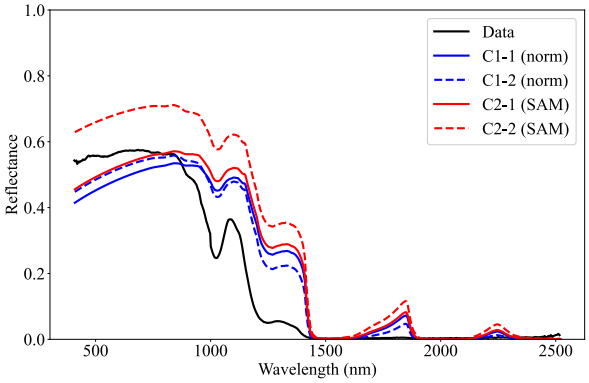

Figure 9. *Spectra obtained from the model used with β and M estimated by cost functions and approaches for the image acquired at $t_1 = 23$ min.*

is actually close to the assumption made by the second approach where both M values are estimated on the first acquisition and kept constant afterwards.

Figure 8 showcases the estimates for the β parameter. In both approaches, SAM is providing values very constants and close to each other. The similarity between the approaches is expected since the M parameter is not changing that much. The constancy of β over time could be related to the evolution of the grain shape that is discussed later. As for $\mathscr{C}_1$, the estimates are increasing along time which is coherent assuming a fixed shape of snow grains. Therefore, grains would expand and sizes would increase. The second approach even estimates higher values. The only drawback is to not have any ground truth for that experiment to qualify those results.

Table 1: Table of estimated parameters that were used for plotting spectra on Figure 9 and Figure 10

	$t_1 = 23$ min		$t_2 = 88$ min	
	β ($\mu m^{1/2}$)	M	β ($\mu m^{1/2}$)	M
C1-1	84.3	$1.53.10^{-6}$	152.4	$4.11.10^{-6}$
C1-2	87.5	$1.34.10^{-6}$	241.1	$1.34.10^{-6}$
C2-1	84.1	$1.51.10^{-6}$	76.8	$1.25.10^{-6}$
C2-2	76.9	$9.41.10^{-7}$	72.8	$9.41.10^{-6}$

In Table 1 were referenced estimated parameters that were used to compute spectra based on Equation (4). Those spectra are displayed on Figure 9 for the acquisition done at $t_1 = 23$ min, and on Figure 10 for the acquisition at $t_2 = 88$ min. The samples at those times were different, but they are quite representative. At t_1, the snow is still present and some areas start to melt. At t_2, the ratio is inversed and the liquid water is predominant in the box. In fact, small snow parts are remaining and flotting. For both times, the temperature was not measured. However, it is not changing much during the overall experiment. In fact, the snow sample might be slighty under 0°C, but then the temperature stabilizes around zero once the melting starts.

There is clearly a difference between the two approaches in term of results. While having a constant concentration of pollutants in the snow, the second approach gives estimates of spectra closer to the spectrum obtained from the data, as it is shown on Figure 10 for C1-1 and C1-2. The choice of cost functions is also to be discussed, as they are providing very different results in the estimate especially for aged snow. The Frobenius norm C_1 is very common and would provide a good estimate of the magnitude while having an appropriate shape of the spectrum. The SAM function C_2 is not subject to the scaling of the reflectance, which suits our data. Since we have a scaling of data for the VNIR camera and one for the SWIR camera, and then a fusion of both data, the border to where is our scaling is unclear. Therefore, the SAM helps discarding those scaling effects and provides a very good shape of the spectrum. In addition, on Figure 7, SAM estimates a value of M in a narrow interval. The estimation is almost constant which is close to the assumption made for the second approach.

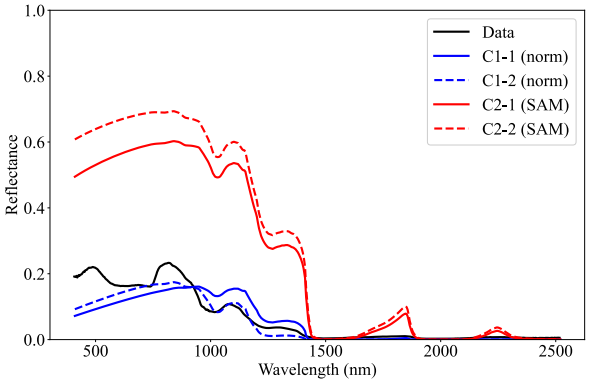

Figure 10. *Spectra obtained from the model used with β and M estimated by cost functions and approaches for the image acquired at $t_2 = 88$ min.*

With the previous results, we would like to introduce an effective parameter $\beta = b\sqrt{d}$ as a parameter to estimate and qualify the snow. This parameter contains the contribution of the snow grain size and the snow grain shape. As pointed out by Picard et al. [20], there are numerous values of the shape factor b depending on the assumption taken. Furthermore, with the snow aging or melting, snow grains will expand leading to a change of shape and size.

On Figure 8, the estimates given by SAM of β remain constant through time. Looking back at the definition of the effective parameter, both the grain size and the grain shape are evolving: one increases while the other decreases. Using Table 2, the estimated value of the snow grain size goes from 328 µm to 767 µm for the same value of the effective parameter. Having a 100% difference just for assuming one shape over the other seems quite important. Therefore, a fixed shape factor does not seem adequate, hence the introduction of the effective parameter β.

Table 2: Table of snow grain sizes depending on the shape assumption. The effective parameter chosen was $\beta = 87.5$ µm$^{1/2}$ for $t_1 = 23$ min.

Grain shape	b	d (µm)
Non sticky sphere	4.44 [20]	388
Cubes	3.39 [20]	666
Long cylinder	4.83 [20]	328
Depth hoar	3.16 [20]	767
Tetrahaedral fractal	3.62 [11]	584

In the case of our experiment, the model presents several limitations. One of them is the assumption of infinte thickness of snow. This cannot be applied for our snow sample due to the proximity of the camera. Also, the model is only considering surface reflections which is suitable for a remote sensing setting. For a close range imaging, the contributions of internal and subsurface reflections need to be added to the model for more accuracy. The problematic is linked to the surface roughness of the snow sample as well.

Conclusion

We conducted an experiment to monitor a melting snow sample using hyperspectral cameras in a controlled environment with known lighting conditions. The data obtained from this experiment in a proximal range was confronted to the Kokhanovsky model, which models the reflectance function of snow using various physical parameters but was developed for remote sensing applications. Therefore, those parameters were estimated through this model. We introduced the effective parameter to describe the contribution of both the snow grain size and the snow grain shape. The computation is ready, but there is a need for more ground truth to verify our results.

We are planning to do a new set of experiments to provide more data to our current set and to compare the results to approve the protocol and model. We are thinking of refining the current protocol as well such as changing the reference tile to increase the signal-to-noise ratio and have better spectra reconstructed. Another possibility for us is to compute our own database for the ice refractive index as it was pointed by Singh et al. [21]. We are also planning to look for other reflectance models of white surfaces (such as the ones that were discarded previously in the introduction), and see if they could fit to the behaviour of the snow. A last aspect would be to conduct the experiment for various geometric configurations (light and camera positions) to have more data for our fitting parameters.

References

[1] T. Aoki, T. Aoki, M. Fukabori, A. Hachikubo, Y. Tachibana, and F. Nishio. Effects of snow physical parameters on spectral albedo and bidirectional reflectance of snow surface. *Journal of Geophysical Research: Atmospheres*, 105(D8):10219–10236, 2000.

[2] T. Carlsen, G. Birnbaum, A. Ehrlich, J. Freitag, G. Heygster, L. Istomina, S. Kipfstuhl, A. Orsi, M. Schäfer, and M. Wendisch. Comparison of different methods to retrieve optical-equivalent snow grain size in central antarctica. *The Cryosphere*, 11(6):2727–2741, 2017.

[3] C. Fierz, R. L. Armstrong, Y. Durand, P. Etchevers, E. Greene, D. M. McClung, K. Nishimura, P. K. Satyawali, and S. A. Sokratov. The international classification of seasonal snow on the ground. resreport, UNESCO-IHP, 2009.

[4] J.-C. Gallet, F. Domine, C. S. Zender, and G. Picard. Measurement of the specific surface area of snow using infrared reflectance in an integrating sphere at 1310 and 1550 nm. *The Cryosphere*, 3(2):167–182, 2009.

[5] G. M. Hale and M. R. Querry. Optical constants of water in the 200-nm to 200-μm wavelength region. *Appl. Opt.*, 12(3):555–563, 1973.

[6] A. A. Kokhanovsky. Reflection of light from particulate media with irregularly shaped particles. *J. Quant. Spectrosc. Radiat. Transfer*, 96(1):1–10, 2005.

[7] A. A. Kokhanovsky. *Light Scattering Reviews: Single and Multiple Light Scattering*, chapter Asymptotic radiative transfer, pages 253–289. Springer Berlin Heidelberg, 2006.

[8] A. A. Kokhanovsky, T. Aoki, A. Hachikubo, M. Hori, and E. P. Zege. Reflective properties of natural snow: approximate asymptotic theory versus in situ measurements. *IEEE Transactions on Geoscience and Remote Sensing*, 43(7):1529–1535, 2005.

[9] A. A. Kokhanovsky and F.-M. Breon. Validation of an analytical snow brdf model using parasol multi-angular and multispectral observations. *IEEE Geoscience and Remote Sensing Letters*, 9(5):928–932, 2012.

[10] A. A. Kokhanovsky, V. V. Rozanov, E. P. Zege, H. Bovensmann, and J. P. Burrows. A semianalytical cloud retrieval algorithm using backscattered radiation in 0.4–2.4 μm spectral region. *Journal of Geophysical Research: Atmospheres*, 108(D1):4008–4026, 2003.

[11] A. A. Kokhanovsky and E. P. Zege. Scattering optics of snow. *Appl Opt*, 43(7):1589–1602, 2004.

[12] L. Kou, D. Labrie, and P. Chylek. Refractive indices of water and ice in the 0.65- to 2.5-μm spectral range. *Appl. Opt.*, 32(19):3531–3540, 1993.

[13] A. Langlois, A. Royer, B. Montpetit, G. Picard, L. Brucker, L. Arnaud, P. Harvey-Collard, M. Fily, and K. Goïta. On the relationship between snow grain morphology and in-situ near infrared calibrated reflectance photographs. *Cold Reg. Sci. Technol.*, 61(1):34–42, 2010.

[14] Q. Libois, G. Picard, J. L. France, L. Arnaud, M. Dumont, C. M. Carmagnola, and M. D. King. Influence of grain shape on light penetration in snow. *The Cryosphere*, 7(6):1803–1818, 2013.

[15] M. Matzl and M. Schneebeli. Measuring specific surface area of snow by near-infrared photography. *J. Glaciol.*, 52(179):558–564, 2006.

[16] E.-A. Milne. Radiative equilibrium in the outer layers of a star. *MNRAS*, 81:361–375, 1921.

[17] B. Montpetit, A. Royer, A. Langlois, P. Cliche, A. Roy, N. Champollion, G. Picard, F. Domine, and R. Obbard. New shortwave infrared albedo measurements for snow specific surface area retrieval. *J. Glaciol.*, 58(211):941–952, 2012.

[18] C. Mätzler. Relation between grain-size and correlation length of snow. *J. Glaciol.*, 48(162):461–466, 2002.

[19] H. S. Negi and A. Kokhanovsky. Retrieval of snow albedo and grain size using reflectance measurements in himalayan basin. *The Cryosphere*, 5(1):2011, 2011.

[20] G. Picard, L. Arnaud, F. Domine, and M. Fily. Determining snow specific surface area from near-infrared reflectance measurements: Numerical study of the influence of grain shape. *Cold Reg. Sci. Technol.*, 56(1):10–17, 2009.

[21] S. Singh, A. Kulkarni, and B. Chaudhary. Hyperspectral analysis of snow reflectance to understand the effects of contamination and grain size. *Ann. Glaciol.*, 51(54):83–88, 2010.

[22] S. G. Warren. Optical constants of ice from the ultraviolet to the microwave. *Appl. Opt.*, 23(8):1206–1225, 1984.

[23] S. G. Warren and R. E. Brandt. Optical constants of ice from the ultraviolet to the microwave: A revised compilation. *Journal of Geophysical Research: Atmospheres*, 113(14), 2008.